Macromolecules

Cite This: Macromolecules 2019, 52, 5860−5871

Article

pubs.acs.org/Macromolecules

Transient-State Rheological Behavior of Poly(ethylene glycol) Diacrylate Hydrogels at High Shear Strain Rates

Ke Luo,[†] Kshitiz Upadhyay,[‡] Ghatu Subhash,[‡] and Douglas E. Spearot*[,†,‡]

[†]Department of Materials Science & Engineering and [‡]Department of Mechanical & Aerospace Engineering, University of Florida, Gainesville, Florida 32603, United States

ABSTRACT: Transient rheological properties of poly(ethylene glycol) diacrylate (PEGDA) hydrogels under Couette flow conditions are determined via molecular dynamics simulations and validated by high strain rate shear experiments. Specifically, the influence of polymer concentration on the transient-state shear-thickening behavior is studied for 20, 25, 50, and 70 wt % PEGDA hydrogels. The transient shear response is characterized by the introduction of dimensionless variables and the application of a self-similar solution to the power-law fluid model. This enables meaningful comparison of the shear-thickening exponent and the transient-state viscosity across the disparate length and time scales between simulations and experiments. The momentum diffusion exponent is found to increase with a decrease in PEGDA concentration, which indicates higher shear-thickening behavior in lower PEGDA concentration hydrogels. Shear-thickening mechanisms in hydrogels are explained by computing the average mesh sizes in the polymer networks and the distributions of junction separations. Two stages of PEGDA chain deformations are observed under shear, where the first stage is associated with chain conformational changes and the second stage is associated with bond length and angular deviations. Hydrogels with lower PEGDA concentration show a faster increase in the average mesh size, which offers higher resistance to shear in both deformation stages, promoting greater shear-thickening behavior.

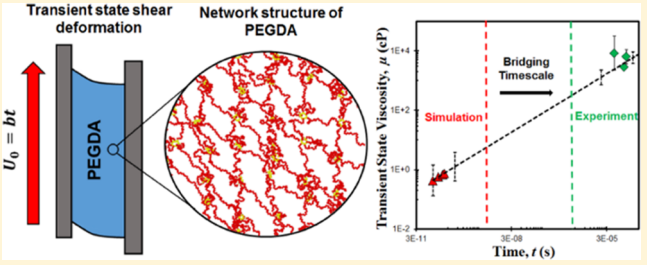

1. INTRODUCTION

Hydrogels are a class of polymeric materials that consist of physically or chemically cross-linked networks swollen in water.[1] They have broad applications in biomedical fields due to their biocompatibility and biodegradability.[2,3] For example, wound dressings made of poly(ethylene glycol) (PEG) hydrogels were shown to promote cell proliferation and wound healing.[4] Space-filling scaffolds made of poly(ethylene glycol) diacrylate (PEGDA) hydrogels were shown to prevent adhesion and internal thickening in tissue-engineered heart valves.[5] In addition, hydrogels are used as surrogate materials for biological tissues in studies where live tissue cannot be used.[6] In these direct and surrogate applications, hydrogels are subjected to a wide range of deformation rates. Therefore, understanding the mechanical behavior of hydrogels under both quasi-static and high strain rate conditions is important. Over the past few decades, several studies have focused on the quasi-static response of hydrogels.[7,8] However, under extreme conditions, such as shock loading characteristic of explosive or ballistic events, these quasi-static studies are not applicable because the behavior of hydrogels is highly rate-dependent.[9−12]

It has been reported via experiments that hydrogels show elevated strength and stiffness at high strain rates ($>10^3$ s^{-1}).[13,14] For example, Subhash et al.[6] conducted high shear rate experiments on ballistic gelatin using a polymer split-Hopkinson pressure bar (SHPB). They characterized the viscosity of gelatins with a power-law fluid model and found that hydrogels have a non-Newtonian behavior with a power-law index of 2.25. Thus, hydrogels have significant shear-thickening behavior, where their viscosity increases with shear strain rate.

Numerous experimental and simulation efforts have been devoted to the investigation of shear-thickening behavior in non-Newtonian fluids. For instance, Hoffman et al.[15] observed that highly concentrated suspensions exhibit shear-thickening behavior, indicated by a discontinuous jump in viscosity at a critical shear stress. Cheng et al.[16] explained this phenomenon as the formation of particle clusters induced by hydrodynamic lubrication forces. Ternik et al.[17] studied the planar flow of concentrated corn scratch solutions using a power-law fluid model, where the solution exhibited shear-thickening behavior with an exponent of 1.15. Zaman et al.[18] conducted nonequilibrium molecular dynamics simulations of Couette flow to investigate the influence of poly(ethylene glycol) (PEG) concentrations on the rheology of silica suspensions. They found that the shear-thickening behavior of the suspension increases with the concentration of PEG. Other theoretical studies developed rheological instability or chaos theory models to interpret shear-thickening behavior.[19,20] In summary, prior research on shear-thickening behavior is mainly conducted on fluids or suspensions. On the other hand, hydrogels, which consist of cross-linked polymer

Received: April 21, 2019
Revised: July 9, 2019
Published: July 26, 2019

DOI: 10.1021/acs.macromol.9b00820
Macromolecules 2019, 52, 5860−5871

networks swollen by a fluid, are different in structure and behavior from the above systems. Therefore, it is necessary to investigate the mechanisms associated with shear-thickening behavior in hydrogels.

Additionally, it is known that the mechanical response of hydrogels is sensitive to water concentration.[21] Yakimets et al.[22] and Subhash et al.[23] investigated the influence of water concentration on the elastic properties of gelatin and agarose gel under quasi-static tensile deformation. The modulus of elasticity was found to decrease with higher water concentration. Richler et al.[13] conducted dynamic compression tests on ballistic gelatin and found that stiffness and strength decrease with higher water concentration. During high strain rate compression, Luo et al.[24] reported that shock pressure and artificial viscosity decrease with higher water concentration in PEGDA hydrogels. Clearly, water concentration has a significant influence on hydrogels, not only in the quasi-static regime but also in the high strain rate regime. However, the above studies focus on tensile and compressive deformations, and it is not yet known how water concentration influences non-Newtonian shear-thickening behavior in hydrogels under high strain rate shear deformation. Therefore, the objective of this work is to characterize the high shear rate transient-state rheology of hydrogels in terms of shear-thickening behavior with a specific focus on the influence of water concentration.

Molecular dynamics (MD) simulation is an effective method to study the atomic-scale structure of materials. It has been extensively used to study non-Newtonian fluid behavior.[25−28] However, because the time and length scales of MD simulations are orders of magnitude different from experiments,[29] previous simulation studies have limited applicability to the existing experimental rheological data. Thus, an important contribution of this work is that the gap between simulations and experiments is bridged by adopting a dimensionless approach proposed by Kwon et al.[30] Instead of measuring the conventional steady-state viscosity, Kwon et al. focused on the transient-state viscosity in planar Couette flow conditions, where the velocity and displacement profiles developed within the shear samples are self-similar. Although this method was originally developed for the analysis of experimental results, it has two advantages to be adopted for the analysis of MD simulation results. First, the self-similarity of transient-state shear momentum diffusion allows the measurement of rheological properties regardless of the spatial or temporal dimensions of the samples. Such dimensionless characteristic overcomes the length/time scale barrier and directly connects experiments and simulations. Second, as Kwon et al.[30] stated, the accuracy of their method depends on the temporal resolution in experiments; MD simulation can improve the accuracy with a nanoscale resolution of shear profiles at nanosecond time intervals. Thus, this study advances the work of Kwon et al.[30] by extending it to MD simulations for the study of non-Newtonian behavior of hydrogels under high strain rate shearing conditions. Transient-state simple shear experiments are conducted using a modified split-Hopkinson pressure bar for the validation of predictions derived from simulation results.

2. CONSTITUTIVE MODELS

Hydrogels are known to behave like non-Newtonian fluids with significant rate-dependent viscous properties. Investigating such behavior requires a constitutive model that describes the relationship between shear rate and viscosity. The power-law model has been used in previous studies to characterize non-Newtonian behavior in fluids.[31] Because of its simplicity, this model is used to study the rheological response of hydrogels. For fluid flow between two parallel plates, the power-law model can be expressed as

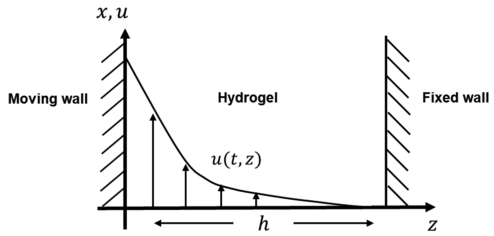

Figure 1. Schematic of transient-state Couette flow in a hydrogel. The velocity profile u is generated by the motion of the left wall.

$$\tau = \alpha \left|\frac{\partial u}{\partial z}\right|^{n-1} \frac{\partial u}{\partial z} \tag{1}$$

where τ is the shear stress, u is the fluid velocity profile in the x-direction, z is the momentum diffusion propagation direction, α is the viscous coefficient, and n describes the degree of non-Newtonian behavior: $n > 1$ represents a shear-thickening fluid and $n < 1$ represents a shear-thinning fluid. The product $\alpha\left|\frac{\partial u}{\partial z}\right|^{n-1}$ is denoted as the viscosity μ. A schematic of transient-state Couette flow is shown in Figure 1. The transient state of the planar Couette flow can be expressed by the incompressible Navier−Stokes equation[32] as

$$\rho\frac{\partial u}{\partial t} = \alpha\frac{\partial}{\partial z}\left[\left|\frac{\partial u}{\partial z}\right|^{n-1}\frac{\partial u}{\partial z}\right] \tag{2}$$

With the boundary conditions

$$\begin{cases} u(0, z) = 0 \\ u(t, 0) = U = bt \\ u(t, h) = 0 \end{cases} \tag{3}$$

where ρ is the material density, b is the acceleration of the moving boundary, U is the velocity of the boundary, and h is the thickness of the sample in the z-direction. When a hydrogel is subjected to the above boundary conditions, a self-similar solution,[33,34] which describes the dimensionless characteristics of the planar Couette flow, can be expressed as

$$\begin{cases} \eta = z/t^k \\ f(\eta) = \dfrac{u(t, z)}{bt} \end{cases} \tag{4}$$

where η is the self-similar variable. Substituting the self-similar solution into eq 2 and solving the equation by separating time-dependent and time-independent variables, the exponent k is found to be $\frac{n}{n+1}$. The detailed solution is provided in ref 30. To apply the self-similar function, the transient-state response is characterized by the momentum diffusion length δ_z

$$\delta_z(t) = \frac{2}{x_d(t, 0)}\int_0^h x_d(t, z)\mathrm{d}z \tag{5}$$

DOI: 10.1021/acs.macromol.9b00820
Macromolecules 2019, 52, 5860−5871

where x_d is the displacement in the x-direction. Then, the momentum diffusion length δ_z is related to time with the self-similar expression

$$\delta_z(t) = c_2\, t^{\nu_z} = c_2 t^{n/n+1} \tag{6}$$

where c_2 is a material constant and ν_z is defined as the momentum diffusion exponent. From eq 6, the shear-thickening exponent n is determined from the dynamic shear profiles during hydrogel deformation. The finite difference method (FDM) is used to solve eq 2 for each time and spatial derivative, after which a histogram is created from the FDM results. The viscous coefficient α is averaged from the highest bin of the histogram, and the viscosity of the hydrogel in the transient state can be determined from the power-law fluid model, as will be done in Section 4.3.

3. SIMULATION AND EXPERIMENTAL METHODS

3.1. Materials and MD Simulation Force Fields. Poly(ethylene glycol) diacrylate with a degree of polymerization of 13 is used, as it has a three-dimensional cross-linked structure and can be swollen to various water concentrations from 30 to 80 wt % to create a hydrogel.[35] Moreover, data is available[36−38] on the equilibrium density and mesh size of PEGDA hydrogels for the validation of the MD simulations. Water molecules in hydrogels are explicitly modeled using the TIP3P flexible potential,[39] and PEGDA polymers are modeled using optimized potentials for liquid simulations (OPLS) united atom potentials.[40] The previous study by Luo et al.[24] showed that this combination of force fields is computationally efficient and predicts less than 2% error in the equilibrium density of PEGDA hydrogels over a range of water concentrations. The atoms in the walls used to impose dynamic shear are arranged in a face-centered cubic crystal structure with (111) surface facing the hydrogel. These atoms are specified as simple Lennard-Jones (LJ) particles with an LJ size parameter of σ = 3.5 Å and an energy parameter of ε = 1.867785 kcal/mol. These parameters provide a lattice parameter of 5.4 Å and a (111) surface energy density of 220 mJ/m^2, which is in the range of a real mica surface.[41] The wall−fluid interaction is calculated from the Lorentz−Berthelot mixing rules. The cutoff distance is set to 10 Å and long-range Coulomb correction is applied with the particle−particle particle−mesh (PPPM) method.

3.2. Construction and Characterization of Hydrogel Networks in MD Simulation. The "perfect network" model is used in many hydrogel studies to describe the structure of an ideal cross-linked network. While this model is different from the real network of a hydrogel, it has shown good agreements with experimental results in elastic modulus, mesh size, and equilibrium density.[42−44] Moreover, the use of the perfect network is a critical step in the development of a transient-state viscosity model for realistic hydrogels with topological variations and defects. Therefore, the perfect network model is used to study dynamic shear conditions in the transient regime. A cross-linked PEGDA junction that consists of six PEGDA chains is created by Moltemplate.[45] One end of each chain is connected at the center of the template cell to form a closed ring structure and the other ends are extended in six directions, as shown in Figure 2a. The junction chemistry and structure can be found in Luo et al.[24] This cross-linked junction is replicated 11 times in the x- and y-directions, and 33 times in the z-direction, as shown in Figure 2b. Water molecules are added to the simulation box after replication to achieve 20, 25, 50, and 70 wt % PEGDA concentrations. The simulation box after water insertion contains approximately 1.5 million atoms. A schematic of a hydrogel model is shown in Figure 2c. The nonuniform set of PEGDA concentrations is selected to allow comparison with dynamic shear experiments, which are only feasible for low PEGDA concentration hydrogels, as will be discussed in Section 4.2. Pure water models with the TIP3P potential are also built for comparison. Equilibration is carried out in the isothermal−isobaric (NPT) ensemble at 298 K and 1 atm for 300 ps. The equilibrium models are 650−700 Å in the z-direction and 200−215 Å in the x- and y-directions depending on the polymer concentration.

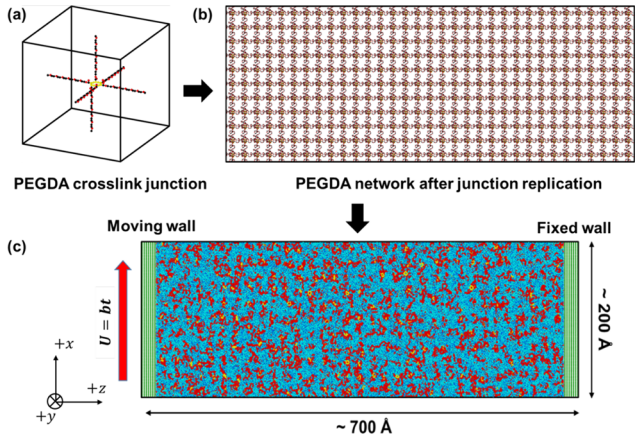

Figure 2. Simulation models of (a) a single PEGDA junction, (b) the PEGDA network after replication, (c) a 50 wt % PEGDA hydrogel model with LJ walls. Green represents LJ atoms, blue represents water molecules, red represents PEGDA chains, and yellow represents cross-linked junctions.

To characterize the cross-linked network of hydrogels, the average mesh size is computed. This is defined as the average length between polymer junctions in a cross-linked network.[46] In experiments, the measurement of mesh size is indirect and mainly based on the assumptions of the Flory−Rehner model,[47] while in simulations, the atomistic details of polymer chains are available. Therefore, the direct measurement of mesh sizes is performed. In this study, the position of a junction is considered to be the geometric center of the junction atoms. The average mesh size is calculated from the end-to-end distance of consecutive junctions in the z-direction.

3.3. Dynamic Shear Deformation in MD Simulation. MD simulations of dynamic shear deformations can be conducted using three different methods:[48] (1) boundary-driven shear, (2) homogeneous shear, and (3) reverse nonequilibrium shear. All of the above methods are capable of capturing steady-state shear deformations. However, as this research focuses specifically on the transient region of shear deformation, only the boundary-driven shear method can satisfy such conditions and thus will be used. To apply the boundary-driven shear method, two LJ walls are placed along the edges of the hydrogel model in the z-direction, as shown in Figure 2. Each wall is 18 Å in thickness and treated as a rigid body. Equilibrium MD simulations are performed in the canonical ensemble (NVT) for 200 ps to relax the distance between walls and hydrogel. Then, to apply boundary conditions commensurate with eq 3, driven velocities with fixed acceleration are applied to the left wall in the positive x-direction, while the position of the right wall is fixed. Dynamic shear deformation is carried out under a constant temperature of 300 K using a Nosé−Hoover-style thermostat.

The displacement and velocity profiles are calculated via a binning method, where the hydrogel model is divided into 100 bins in the z-direction. Each bin has around 10 000 atoms for the calculation of average bin displacement and velocity. After obtaining transient wave propagation profiles, the momentum diffusion length is calculated from eq 6. All simulation results presented in this paper are averages over three independent hydrogel models with different initial configurations. All MD simulations are performed using the LAMMPS code.[49]

3.4. Material Preparation in Experiment. PEGDA ($\bar{M}_n \approx 700$; degree of polymerization = 13), free-radical initiator ammonium persulfate (APS), and accelerator *N*,*N*,*N*′,*N*′-tetramethylethylenediamine (TEMED) are purchased from Sigma-Aldrich (Milwaukee, WI). Ultrapure water is produced by a Milli-Q water purification system (Millipore Corporation, Bedford, MA). Hydrogel specimens are prepared by first dissolving PEGDA in ultrapure water to obtain

DOI: 10.1021/acs.macromol.9b00820
Macromolecules 2019, 52, 5860−5871

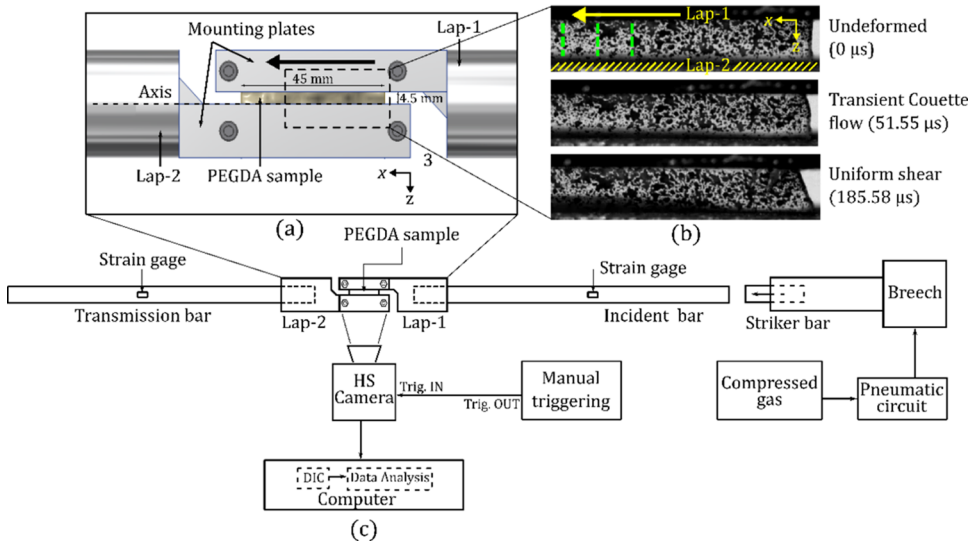

Figure 3. (a) Front view of the single-lap simple shear test fixture, which consists of two laps and two mounting plates securing the specimen. (b) High-speed images of the specimen at different times during the test, showing transient Couette flow and uniform shear stages. (c) Schematic of the modified split-Hopkinson pressure bar setup.

different polymer concentrations (20, 25, and 50 wt %); the resulting mixture is then sonicated for 1 h until a clear solution is obtained. APS and TEMED are added to this solution for chemical cross-linking. Concentrations of 0.1, 0.15, and 0.25 wt % APS are used for the 20, 25, and 50 wt % PEGDA samples, respectively, whereas a fixed concentration of 0.1 wt % TEMED is used for all samples. The resulting mixture is poured into rectangular poly(methyl methacrylate) molds (45 mm x 30 mm x 3.5 mm) for polymerization, which takes several hours to complete depending on the PEGDA concentration in the prepolymerization mixture. The samples are then taken out of the molds and kept in ultrapure water. Insignificant volume changes (<3 wt %) are noticed in the samples after storage, which concurs with previously reported PEGDA13 results in Ju et al.[35] Dynamic shear experiments are conducted within 5 min of taking the samples out of the ultrapure water.

3.5. Dynamic Shear Experimental Setup. A previous study by the authors[50] developed an approach to perform simple shear experiments on polydimethylsiloxane at high strain rates using a modified split-Hopkinson pressure bar (SHPB) setup. This experimental approach is adopted in this work to investigate the shear-thickening behavior in PEGDA hydrogels. Figure 3c shows a schematic of the modified SHPB setup, which consists of two long cylindrical maraging steel incident and transmission pressure bars (with centrally bonded strain gages), a short (6 in) striker bar, and a single-lap shear fixture that is housed between the two pressure bars through its hollow ends (see Figure 3a). A PEGDA hydrogel specimen plate (45 mm × 30 mm × 3.5 mm) is placed between the two lap plates (Lap-1 and Lap-2) of the shear fixture and is secured in place using two mounting plates. This ensures that the gage section experiences simple shear when Lap-1 translates relative to Lap-2. Note that a low clamping force is maintained by controlling screw thread rotation to prevent any damage to the specimen. The specimen gage section (4.5 mm width) is speckled by a fine black spray paint (100−300 μm, Krylon Products Group, Cleveland, OH) for strain analysis using the digital image correlation (DIC) method. A high-speed camera (Phantom v710, Vision Research, Inc., Wayne, NJ) is used to capture the deformation. Three tests are conducted for each polymer concentration (20, 25, and 50 wt %).

To start the experiment, pressurized nitrogen from a compressed gas cylinder is used to launch the striker bar toward the incident bar; the resulting impact generates a compressive stress wave. This stress wave upon reaching the incident bar end imparts a high-velocity input to Lap-1, which linearly increases for a short time before becoming nearly constant for the duration of the test.[50] Note that Lap-2 remains stationary during this deformation owing to the very low impedance of PEGDA as compared to the metallic bars. The fixture dimensions are such that both the shear plane and center plane along the sample thickness pass through the force transducer axis, eliminating any unwanted bending moment. To capture the transient Couette flow in the early part of the shear deformation, the high-speed camera is manually triggered through a 5 V transistor−transistor logic pulse. For the 20 and 25 wt % PEGDA samples, the camera is set to capture deformation images at 97 000 frames per second (fps; one image every 10.31 μs with an exposure time of 6.3 μs). This yields a 512 × 128 pixel resolution and a ∼21 pixels/mm spatial resolution such that around 95 pixels exist along the specimen gage section width. For the stiffer 50 wt % PEGDA samples with a much shorter transient Couette flow duration, the imaging frequency is raised to 180 000 fps (one image every 5.55 μs with an exposure time of 5.06 μs). Increasing the temporal resolution, however, decreases the pixel resolution to 192 × 104 and spatial resolution to ∼15 pixels/mm such that there are about 68 pixels across the gage section width. Captured images are analyzed using the commercial two-dimensional (2D) DIC Vic-2D 6 software (Correlated Solutions, Inc., Irmo, SC) to measure the deformation and velocity fields; subset size is selected for individual imaging data based on the speckle density and speckle size (subset size of > (3 × speckle size)) and also the sigma value (one standard deviation confidence interval) of the subset tracking function. Note that the strain signals from strain gages on the SHPB are not utilized. The role of the SHPB apparatus in this test is to impart a linearly increasing velocity to the upper lap plate (Lap-1) of the single-lap shear fixture during the transient deformation stage in the high strain rate shear experiment. The SHPB provides a means to generate the necessary boundary conditions for the implementation of the self-similar solution and the development of a transient-state shear model for hydrogels.

Figure 3b shows high-speed images of a typical PEGDA specimen under simple shear deformation, which consists of a viscoelastic transient Couette flow stage that leads to uniform simple shear deformation. Three line segments (marked as green broken lines in Figure 3b) in the central region of the specimen are analyzed for each sample to study the average one-dimensional transient Couette flow. Consistent with the MD simulation setup (Figure 2), the x- and z-directions correspond to the shearing and momentum diffusion directions, respectively. The displacement field along individual line segments yielded by 2D DIC is used to calculate the momentum diffusion length via eq 5 and the shear-stiffening exponent using eq 6. Only the time domain starting from t = 0 (initiation of displacement)

DOI: 10.1021/acs.macromol.9b00820
Macromolecules 2019, 52, 5860−5871

up to $t = t_0$ is considered, the latter being the time up to which the velocity input is linear. Further, the time and spatial derivatives of the displacement field are computed using the finite difference method to numerically solve the incompressible Navier–Stokes equation given in eq 2, identical to that done in MD simulations, which further results in the transient-state viscosity μ in the experimental time scale using the relation $\mu = \alpha \left|\frac{\partial u}{\partial z}\right|^{n-1}$. For additional details regarding the high strain rate simple shear experiment, the reader is referred to the authors' previous publication.[50]

4. SIMULATION AND EXPERIMENTAL RESULTS

4.1. Validation of Boundary Conditions and Self-Similar Solution in MD Simulations. The boundary-driven shear method provides a simulation design that is similar to experiments, but it is limited to a maximum boundary velocity due to slippage that may occur at the interface between the hydrogel and walls.[48] To understand the influence of slippage on the shear simulation, the displacement profiles of 50 wt % PEGDA hydrogels under accelerations of 1×10^{12}, 2×10^{12}, and 4×10^{12} m/s^2 at 100 ps are plotted in Figure 4. In the displacement profiles, the first 18 Å in the z-direction represents the moving LJ wall, while the remaining represents momentum diffusion in the hydrogel samples. In this study, the surface velocity of a PEGDA hydrogel is approximated as the velocity of the first bin of the hydrogel profile. Slippage is clearly observed as the difference in displacement between the hydrogel surface and the LJ wall, where the magnitude of slippage increases with acceleration. This is because the acceleration of the LJ wall creates a traction force that exceeds the maximum force of interaction between the hydrogel and the LJ wall, defined by the LJ parameters. To further understand the influence of slippage on the shape of the displacement profiles, all displacements are normalized by the maximum displacement of the hydrogel at the interface with the wall. The normalized profiles are shown in the inset of Figure 4. Clearly, the normalized profiles are identical under the three accelerations considered. Such an observation suggests that the shape of the momentum diffusion profile is independent of the level of slippage, as well as the acceleration. Based on the displacement profile, the momentum diffusion length δ_z for each acceleration at 100 ps is calculated from eq 5 and shown as the length between dotted lines in Figure 4. The same momentum diffusion length is obtained for all chosen accelerations.

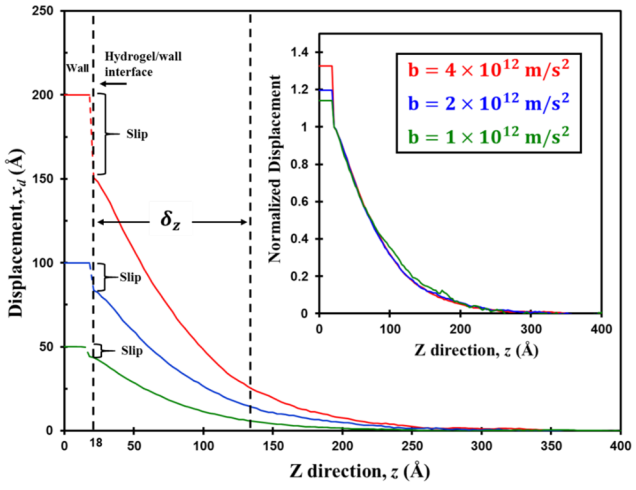

Figure 4. Displacement profiles from the MD simulation of 50 wt % PEGDA hydrogels under accelerations of 1×10^{12}, 2×10^{12}, and 4×10^{12} m/s^2 at 100 ps. The left dotted line represents the maximum displacement of the hydrogel at the wall–hydrogel interface. The dotted lines indicate the momentum diffusion length at 100 ps. The inset reveals normalized displacement profiles at the above accelerations.

The self-similar solution requires constant acceleration at the boundary; thus, it is important to examine the influence of slippage on the boundary velocity. Figure 5 shows the velocities of the moving wall and the 50 wt % PEGDA hydrogel surface at accelerations of 0.5×10^{12}, 1×10^{12}, 2×10^{12}, and 4×10^{12} m/s^2 as a function of simulation time. The imposed velocity of the moving wall is clearly identified as a straight line. However, the velocity of the hydrogel surface is slower than the wall at each acceleration, which is the result of slippage at the hydrogel/wall interface. At each acceleration, the velocity of the hydrogel surface exhibits a linearly increasing region at the beginning of the acceleration. This linear region slowly decays with time due to increased slippage at the interface, and the time duration of the linear velocity region decreases with increasing acceleration. For an acceleration of 0.5×10^{12} m/s^2, the velocity profile of 50 wt % PEGDA hydrogel closely follows the wall for 400 ps and hence is treated as a linear profile. This provides the upper time limit that maintains the mandatory boundary condition in eq 3 for the measurement of momentum diffusion lengths.

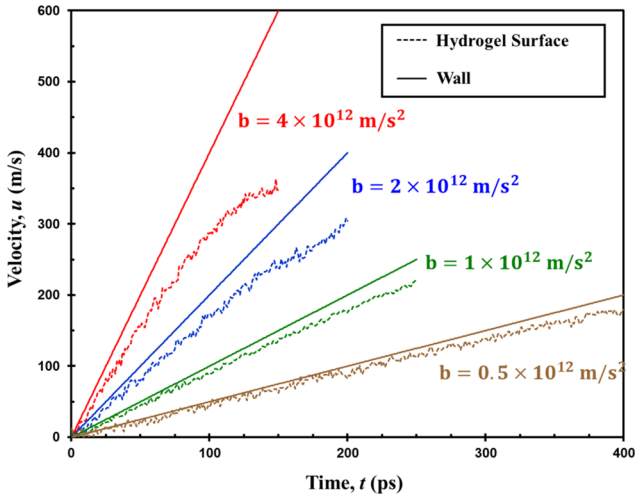

Figure 5. Velocity profiles from the MD simulation of the moving wall and the surface of 50 wt % PEGDA hydrogel at accelerations of 0.5×10^{12}, 1×10^{12}, 2×10^{12}, and 4×10^{12} m/s^2.

The self-similar solution assumes that the shape of the displacement or velocity profile is self-similar and independent of time when the thickness of hydrogel is considered as semi-infinite. To confirm this assumption, Figure 6 shows a plot of the evolution of displacement profiles in 50 wt % PEGDA hydrogels at 0.2, 0.3, and 0.4 ns under an acceleration of 0.5×10^{12} m/s^2. As time evolves, the momentum diffuses in the z-direction. The displacement profile at each time step is then used in eq 4 to calculate the self-similar function $f(\eta)$, as shown in the inset of Figure 6. Self-similar functions are found to be consistent at any time during the simulation. Combining this observation with the previous results in Figure 4, the self-similar solution is validated, as it is independent of time and acceleration in the MD simulations.

4.2. Validation of Experimental Setup. Figure 7a,c, and d show the characteristic evolution of shear displacement profiles with time obtained from the 2D DIC analysis of high strain rate shear deformation in 20, 25, and 50 wt % PEGDA hydrogels, respectively. Figure 7b shows the deformation images and full-field horizontal displacement maps of a 20 wt % hydrogel sample corresponding to different time steps highlighted in Figure 7a. The area of interest for every sample is a ~2.5 mm wide region in the central part of the hydrogel where edge effects due to mounting constraints are minimum.[50]

By comparing the evolution of displacement profiles in the three investigated polymer concentrations, it is noted that the momentum

DOI: 10.1021/acs.macromol.9b00820
Macromolecules 2019, 52, 5860–5871

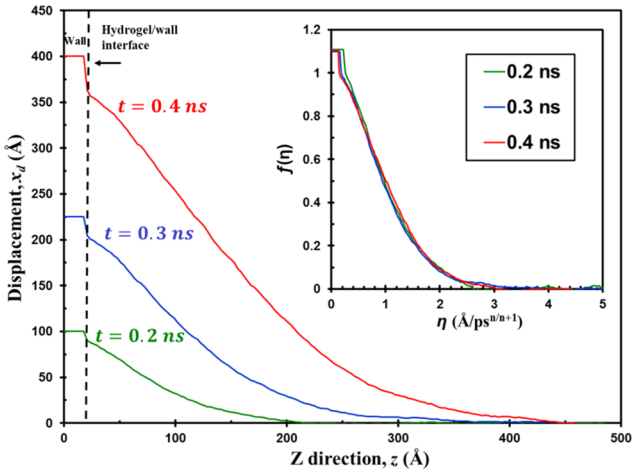

Figure 6. Displacement profiles from the MD simulation of 50 wt % hydrogel at 200, 300, and 400 ps under 0.5 × 10^{12} m/s^2 acceleration. The inset shows the self-similar function $f(\eta)$ at the above times.

diffusion speed increases with an increase in polymer concentration. For the momentum to diffuse 2 mm in the z-direction, it takes ∼120, ∼40, and ∼20 μs in 20, 25, and 50 wt % PEGDA samples, respectively; at the same time, the wall displacements (x_d) for these hydrogel samples are ∼0.55, ∼0.07, and ∼0.035 mm, respectively. The higher momentum diffusion speed in greater polymer concentration samples limits the number of displacement profiles that can be extracted and also results in a very small wall displacement (boundary at z = 0) by the time the diffusion is completed. This also limits the ability to capture good DIC images due to the limited time available to capture the deformation at sufficiently high resolution. The combined effect of these two factors (fewer displacement profiles and small wall displacement) gives an uncharacteristic shape of the displacement profiles of 50 wt % PEGDA samples (Figure 7d) from an ideal one (Figure 1). While this has limited influence on the shear-thickening exponent calculation, the errors are aggravated when higher-order time and spatial derivatives of the displacement fields are computed for the estimation of the transient-state viscosity. Thus, as will be presented in the next section, while the shear-thickening exponent is calculated for all of the three hydrogel concentrations considered in the experiments, only the displacement profiles of 20 and 25 wt % hydrogels are considered for the calculation of the transient-state viscosity.

4.3. Characterization of Shear-Thickening Behavior. In the power-law fluid model, the characterization of shear-thickening behavior requires two variables: the shear-thickening exponent n and the viscous coefficient α. Their characteristics are discussed separately in this section.

The shear-thickening exponent n is characterized by the relationship between momentum diffusion length and time, based on eq 6. Such a characterization is derived from the self-similar solution in Section 2. Thus, the shear-thickening exponent is innately dimensionless and consistent in any time or length domains. Figure 8 plots the momentum diffusion length versus time for 20, 25, 50, and 70 wt % PEGDA hydrogels and water from MD simulations in logarithmic scale. A general power-law fit is applied to the data. Note that the error bars in the calculation of momentum diffusion length increase with water concentration. This result can be explained by the higher fluctuations of water molecules compared to those of the polymer network. Such statistical fluctuation leads to increased oscillation in velocity and displacement profiles, which results in errors in the momentum diffusion length measurement. Moreover, the errors are found to decrease at longer time duration. The large scatter at an early time is due to the relatively small shear displacement compared to the displacement associated with thermal oscillation. Such an error decreases with time because the magnitude of shear displacement increases. Thus, similar to the linear velocity region defining the upper bound in the measurement of momentum diffusion length (Figure 5), the thermal oscillations control the lower bound. Thus, to report results with higher accuracy, this study calculates the momentum diffusion length starting after 100 ps, where the errors of all measurements are below 10%.

In Figure 8, hydrogels with higher polymer concentration show longer momentum diffusion length at each time during the shear deformation, which concurs with the experimental observation in Figure 7 that the momentum diffusion speed increases with polymer

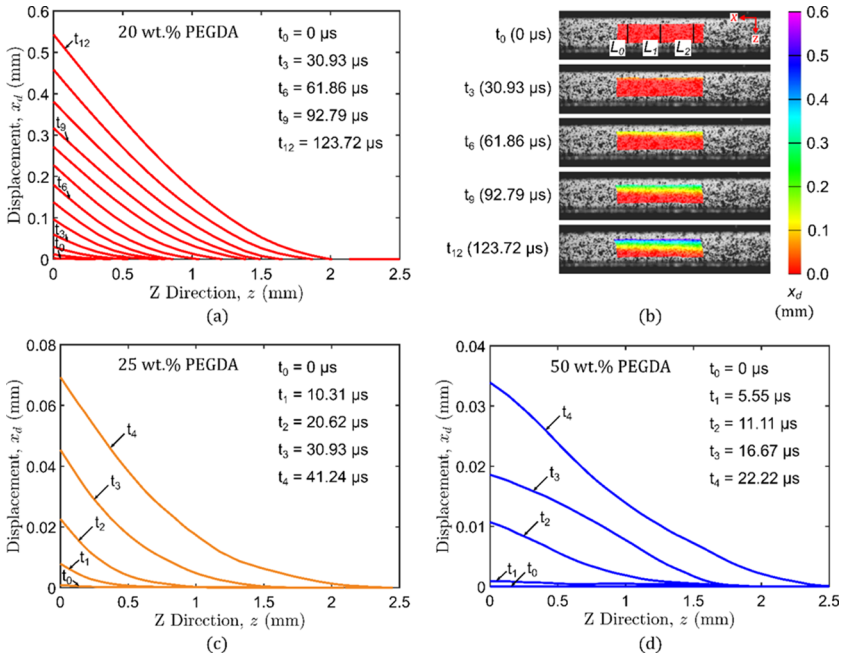

Figure 7. Experimental results of (a) evolution of the displacement profile of 20 wt % PEGDA hydrogels and (b) the corresponding high-speed images at various time steps illustrating the transient phase of shear deformation. Displacement profiles of (c) 25 wt % and (d) 50 wt % PEGDA hydrogels at various time steps during the dynamic shear experiment.

DOI: 10.1021/acs.macromol.9b00820
Macromolecules 2019, 52, 5860−5871

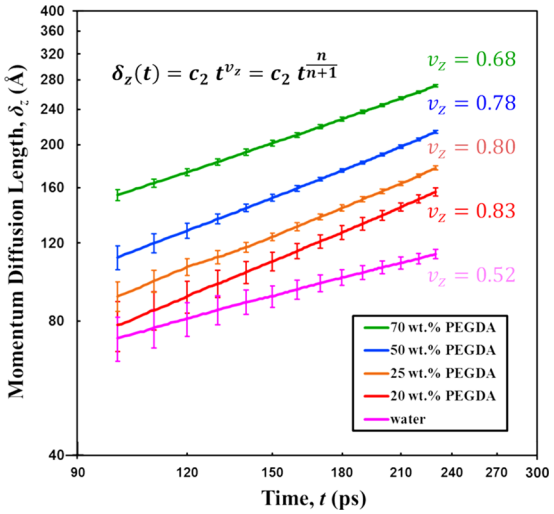

Figure 8. Simulation results of the momentum diffusion length versus time for 20, 25, 50, and 70 wt % PEGDA hydrogels.

concentration. Additionally, the slope of each power-law curve is the momentum diffusion exponent in the form of $v_z = \frac{n}{n+1} = \partial \log \delta_z / \partial \log t$, based on eq 6. As shown in Figure 8, when the PEGDA concentration increases, the momentum diffusion exponent decreases. However, water exhibits the opposite trend than PEGDA hydrogels, as it has the lowest momentum diffusion exponent. This is because the diffusion mechanisms are different in water and hydrogels. In water, the momentum is transferred through the intermolecular collisions of water molecules, while in hydrogels, the momentum diffusion is controlled by the intramolecular forces in the cross-linked network; this aspect will be further discussed in Section 5.

The shear-thickening exponent for different hydrogels is calculated as $n = \frac{v_z}{1 - v_z}$ according to eq 6. The calculated shear-thickening exponents from MD simulations are summarized in Table 1. Comparison to experimental results is also provided. The water models have the lowest shear-thickening exponent of 1.07, which agrees well with the experimental observation of water as a Newtonian fluid with a shear-thickening exponent of unity.[51] As the PEGDA concentration increases, the hydrogels exhibit a decreasing trend in the shear-thickening exponent. Simulations predict that a 20 wt % PEGDA hydrogel exhibits the highest shear-thickening behavior with n = 4.79 and a 70 wt % PEGDA hydrogel has the lowest exponent of 2.18. This trend is consistent with the experimentally obtained shear-thickening exponents for 20, 25, and 50% wt % PEGDA hydrogels, which also decrease with increasing polymer concentration. However, simulations overpredict the shear-thickening exponents when compared to experiments. This overprediction may due to the simulation and experimental errors associated with the measurement of displacement profiles and the momentum diffusion lengths. It could also be related to the behavior of the perfect network used in these simulations, which has higher average connectivity than a network in a typical hydrogel. Studies have shown that the network topology of cross-linked materials can influence their mechanical behaviors.[52−54] For example, polymers with a low degree of cross-link connectivity commonly have low elastic moduli at low strain rates, while at high strain rates, the influence network connectivity is less critical[52] due to the time scale of the loading relative to the time scales associated with polymer chain relaxations. However, a complete understanding of how network topology affects the shear response of hydrogels under high strain rate conditions is not yet understood. Thus, the variation of network topology could be a focus of future investigations of the transient-state shear-thickening behavior in hydrogels.

In contrast to the dimensionless shear-thickening exponent, the viscous coefficient α is dimensional as it is a scaling variable that describes the magnitude of dynamic viscosity.[55] According to eq 2, α is dependent on the time rate of change of the velocity $\frac{\partial u}{\partial t}$, shear-thickening exponent n, and velocity profile $\frac{\partial u}{\partial z}$. Since all variables in eq 2 are known, the viscous coefficient can be directly calculated for hydrogels and water; this data is presented in Table 2. The dimensionless diffusion coefficient also provided in Table 2 will be discussed later in this section.

From Table 2, hydrogels have distinctly different magnitudes of the viscous coefficient. Moreover, the direct comparison of viscous coefficient between simulations and experiments is not appropriate because the viscous coefficient is dimension and acceleration-dependent. In particular, simulations are carried out under accelerations of ~10^{12} m/s^2, and the experimental accelerations in this research are on the order of 10^5−10^6 m/s^2. Such a large gap in acceleration will lead to different magnitudes of viscous coefficient computed from simulation and experimental data. To characterize the viscous properties in acceleration-independent conditions, the following dimensionless variables are introduced

$$\bar{z} = \frac{z}{\delta_z(t_0)},\ \bar{u} = \frac{u}{U_0},\ \bar{t} = \frac{t}{t_0} \tag{7}$$

Here, t_0 is defined as the time when the maximum velocity U_0 is reached. Substituting the variables defined in eq 7 into eq 2, the fluid flow equation becomes independent of time or length scale

$$\frac{\partial \bar{u}}{\partial \bar{t}} = D\frac{\partial}{\partial \bar{z}}\left[\left|\frac{\partial \bar{u}}{\partial \bar{z}}\right|^{n-1}\frac{\partial \bar{u}}{\partial \bar{z}}\right] \tag{8}$$

Here, D is the dimensionless diffusion coefficient, which is a material constant that can be directly solved from eq 8 with the same method as the calculation of α. The relationship between α and D can be expressed as

$$\alpha = \frac{DC_2^{n+1}\rho}{b^{n-1}} \tag{9}$$

Equation 9 explains the strong acceleration dependence of the viscous coefficient. Note that in the transient state of shear deformation, the hydrogel is subject to different shear strain rates depending on the position in the z-direction, as shown in Figure 1. The highest shear rate occurs at the hydrogel surface while it slowly decreases to zero with increasing z. Thus, the shear strain rate of hydrogels is defined as the maximum shear rate $\frac{U_0}{\delta_z}$ at the surface. Substituting the shear rate into eq 1, the transient-state viscosity of the material is rewritten as

$$\mu = D\rho\, C_2^2 t_0^{n-1/n+1} \tag{10}$$

where μ is the transient-state viscosity and t_0 is the total duration of the transient state. According to eq 10, the transient-state viscosity of a Newtonian fluid such as water is a constant regardless of the time, while the transient-state viscosity of a non-Newtonian fluid is time-dependent. Figure 9 shows the transient-state viscosity of 20, 25, 50, and 70 wt % PEGDA hydrogels obtained by MD simulations, along with experimentally obtained values of 20 and 25 wt % samples. The simulation results are extrapolated to the experimental time regime on

Table 1. Shear-Thickening Exponents (n) of PEGDA Hydrogels from Simulation and Experiment

	water	20 wt % PEGDA	25 wt % PEGDA	50 wt % PEGDA	70 wt % PEGDA
Simulation	1.07 (0.93−1.22)	4.79 (3.45−7.69)	3.93 (3.41−4.35)	3.49 (2.96−3.80)	2.18 (1.89−2.23)
Experiment	1.00[51]	3.65 (2.55−5.76)	2.82 (1.98−4.32)	2.11 (1.52−3.06)	N/A

DOI: 10.1021/acs.macromol.9b00820
Macromolecules 2019, 52, 5860−5871

Table 2. Coefficients of Power-Law Fluid Model for PEGDA Hydrogels

	20 wt % PEGDA	25 wt % PEGDA	50 wt % PEGDA	70 wt % PEGDA
Viscous coefficient, α kg × s^{n-2}/m	$3.37 \times 10^{-42} \pm 1.8 \times 10^{-43}$	$1.14 \times 10^{-33} \pm 3.76 \times 10^{-34}$	$2.58 \times 10^{-29} \pm 9.8 \times 10^{-31}$	$2.17 \times 10^{-16} \pm 1.5 \times 10^{-17}$
Dimensionless diffusion coefficient, D	0.711 ± 0.004	0.264 ± 0.001	0.081 ± 0.003	0.038 ± 0.002

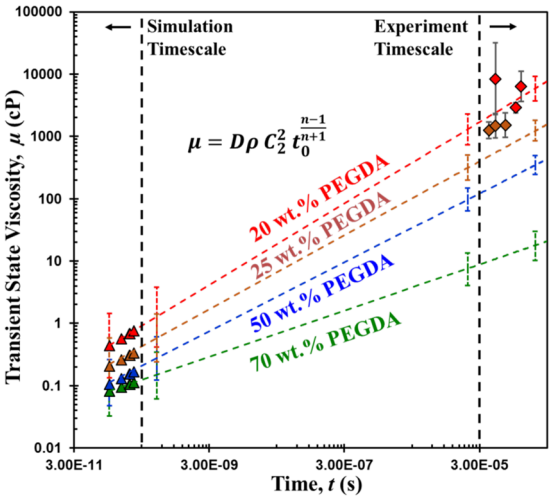

Figure 9. Simulation and experimental results of transient-state viscosity versus time for 20, 25, 50, and 70 wt % PEGDA hydrogels. Triangles represent MD simulation results, the dashed lines represented the extrapolated prediction to experimental time scale, and diamonds represent experiment data.

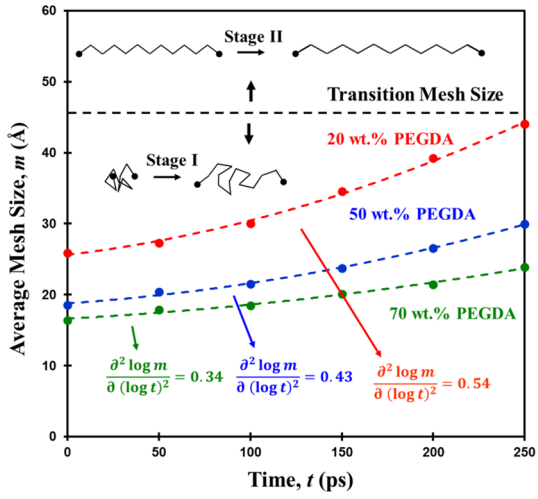

Figure 10. MD simulation data showing the time evolution of average mesh size in 20, 50, and 70 wt % PEGDA hydrogels and schematic depiction of stage I and stage II deformations.

the order of 10^{-5} s. According to the experimental results, 20 wt % PEGDA hydrogels show a transient-state viscosity of 5373 cP at 93 μs and 25 wt % PEGDA hydrogels exhibit an average of 1420 cP at 55 μs when averaged over three tests. This result concurs with the trend predicted from atomistic simulation that the transient-state viscosity decreases in higher polymer concentrations. Note that 50 and 70 wt % samples are not considered in the estimation of the transient-state viscosity because of the imaging and DIC resolution issues for higher polymer concentrations due to faster momentum diffusion speeds, as described in Section 4.2. Equation 10 and Figure 9 are major outcomes of this study, as they relate dimensionless constants with the dimensional material properties and directly connect experimental and simulation time regimes.

5. EVOLUTION OF HYDROGEL NETWORKS DURING SHEAR DEFORMATION

5.1. Characterization of Cross-Linked Networks in Hydrogels. The cross-linked network is the distinct feature of a hydrogel that controls its mechanical response,[8] and MD simulation provides a clear view of network evolution during shear. To characterize the deformation and evolution of the hydrogel network in the transient shear state, the average mesh size m in the transient region where $z \leq \delta_z$ in 20, 50, and 70 wt % PEGDA hydrogels is calculated and shown in Figure 10. Second-order polynomial fits are applied to describe the mesh size trends. The variation for each data point is below 5%. At 0 ps, when hydrogels are at an equilibrium state, the average mesh sizes for all hydrogels agree with experimental data.[35] Larger average mesh sizes are observed in lower-PEGDA-concentration hydrogels because of the swelling effect.[56] As the deformation progresses, at 250 ps, hydrogels with lower PEGDA concentration show a faster increasing rate in the average mesh size. The rate of mesh size increase is calculated as $\frac{\partial^2 \log m}{\partial (\log t)^2}$. To interpret the trend of mesh size in terms of shear-thickening behavior, it is necessary to investigate the mechanism of network deformation in the hydrogel.

It is reported[38,57−59] that the deformation of hydrogel networks consists of two stages: stage one shows viscoelastic behavior that involves conformational changes of polymer chains, such as rotations, while the bond and angle distribution remain unchanged; stage two starts when the polymer chain has uncoiled. Further elongation of a polymer chain requires bond and angle stretching, which have a higher resistance than the conformation changes. To differentiate between the two deformation regimes, the transition mesh size is computed as the length when a polymer chain is at its longest conformation, while its bond and angles are in the equilibrium state. When the junction separation distance exceeds the transition mesh size, the deformation mechanism of that chain transitions from stage one to stage two, as depicted in Figure 10. In this study, all PEGDA hydrogels have the same composition with the degree of polymerization of 13; thus, for this polymerization, the transition mesh size for PEGDA13 is estimated as 46.64 Å using a bond distance of 1.46 Å and an average angle of 110°.[40] In Figure 10, the average mesh sizes at all concentrations are lower than the transition mesh size even after deformation for 250 ps. This indicates that hydrogels are mainly subject to stage-one deformation. Furthermore, the faster rate of increasing mesh size in lower PEGDA concentrations indicates a higher viscoelastic resistance from chain uncoiling. This resistance results in higher transient-state viscosity and higher shear-thickening behavior in the lower PEGDA concentration hydrogel, which explains the observations presented in Figures 8 and 9.

To further understand the role of average mesh size and junction separation distance on the shear-thickening behavior of hydrogels, the distribution of junction separations for 20, 50, and 70 wt % PEGDA hydrogels at 0 and 250 ps is shown in Figure 11. At 0 ps, junction separation is lower than the transition mesh size for all concentrations of the hydrogel. As

DOI: 10.1021/acs.macromol.9b00820
Macromolecules 2019, 52, 5860−5871

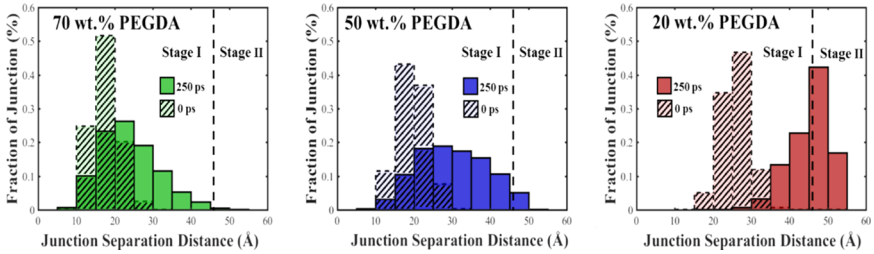

Figure 11. MD simulation results of the distribution of junction separation distance for PEGDA hydrogels at 0 and after deformation at 250 ps. The dotted line is the transition mesh size of PEGDA with polymerization of 13.

time increases, the distribution shift for 20 wt % PEGDA hydrogel is larger than that for 50 and 70 wt % PEGDA hydrogels due to the faster increasing rate of the average mesh size. At 250 ps, more than 45% of the PEGDA chains in the 20 wt % PEGDA hydrogel have exceeded the transition mesh size. Those chains exhibit stage-two deformation, which has a higher resistance to deformation and hence higher shear-thickening behavior. In comparison, for 50 and 70 wt % PEGDA hydrogels, less than 10% of chains have crossed the transition mesh size. Thus, less shear-thickening behavior is observed. This statement is further confirmed by visually comparing the network structure of 20 and 50 wt % PEGDA hydrogels in Figure 12. Chains within the region where $y \leq 20$ Å are shown to represent the hydrogel network. At 250 ps, polymer chains in 20 wt % PEGDA hydrogels are extensively stretched within the momentum diffusion region. In contrast, coiled chains are still dominant in 70 wt % PEGDA hydrogels. The above analysis reaffirms the conclusion that shear-thickening behavior in hydrogels stems from the rate at which the mesh size increases during deformation. In the stage-one deformation, a faster increase of average mesh size promotes higher resistance from the conformation changes and allows more chains to exceed the transition mesh size resulting in stage-two resistance. Both situations lead to higher shear-thickening behavior in hydrogels.

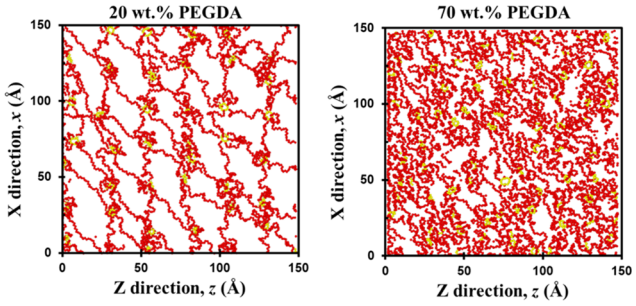

Figure 12. MD simulation network structures of PEGDA hydrogel at 250 ps. Red represents PEGDA chains and yellow represents cross-link junctions. Chains within $y \leq 20$ Å region are shown.

5.2. Influence of PEGDA Concentration on the Mesh Size Evolution. The previous section discussed the shear-thickening behavior of hydrogels in terms of average mesh size and junction separation distance. As the objective of this research is to understand the influence of polymer concentration on the shear-thickening behavior, it is necessary to relate the network structure of hydrogel with polymer concentration. Accordingly, two variables are introduced: the arc length of displacement (L_d) and the cumulative mesh size (m_c). The arc length of displacement is defined as the length of the curve in the displacement profile within the momentum diffusion region, as shown in Figure 13a. It is directly controlled by the momentum diffusion exponent. As shown in Figure 8, the momentum diffusion exponent is a function of PEGDA concentration. Therefore, the arc length of displacement is also directly dependent on polymer concentration. The cumulative mesh size, m_c, on the other hand, is defined as the summation of lengths between consecutive junctions that are connected in the z-direction within the momentum diffusion region, as shown in Figure 13b. It is a direct representation of network structure in the transient region. It is expressed as

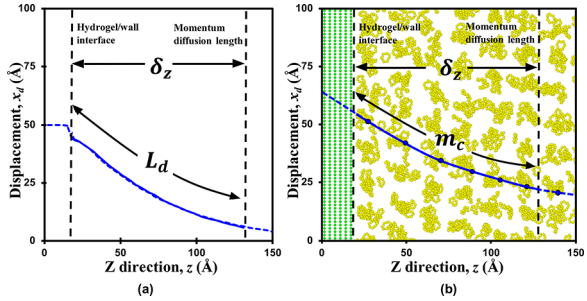

Figure 13. MD simulation results for (a) the displacement profile of 50 wt % PEGDA at 100 ps. The arrows indicate the arc length of displacement. (b) Snapshot of the 50 wt % PEGDA hydrogel model at 100 ps; green represents atoms of LJ walls, yellow represents atoms in cross-link junctions, and blue dots represent geometric centers of cross-link junction. The arrows indicate the cumulative mesh size.

$$m_c = \frac{m}{m_0}\delta_z(t) \tag{11}$$

where m_0 is the average mesh size in an equilibrium state. Both variables describe the current state of deformation in a hydrogel, where the arc length of displacement is based on the average movement of all atoms, while the cumulative mesh size is only derived from the movement of cross-link junctions. In a hydrogel, the displacement should be adequately reflected at the microstructure level, such as the average mesh size. Thus, the arc length of displacement should be equal to the cumulative mesh size as

$$L_d = m_c = \frac{m}{m_0}\delta_z(t) \tag{12}$$

To verify eq 12, the arc length of displacement measured by the trapezoidal rule and the cumulative mesh size calculated from eq 11 are plotted with time in Figure 14. Good agreement is found between the two quantities for three PEGDA concentrations, which validates the above discussion. Furthermore, as shown in Figure 14, the arc length of displacement is larger in higher-PEGDA-concentration hydro-

DOI: 10.1021/acs.macromol.9b00820
Macromolecules 2019, 52, 5860−5871

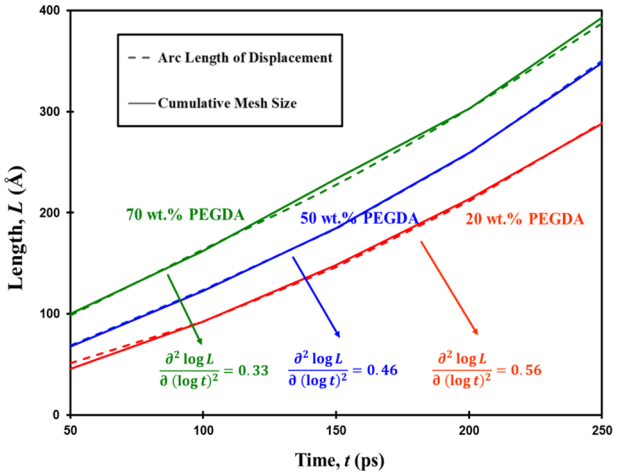

Figure 14. Evolution of the arc length of displacement (dotted line) and cumulative mesh size (solid line) for 20, 50, and 70 wt % PEGDA hydrogels via MD simulation.

gels, which again illustrates its concentration dependence. Rewriting eq 12 in a log–log scale and taking the second derivative with respect to log t

$$\frac{\partial^2 \log L_d}{\partial (\log t)^2} = \frac{\partial^2 \log m}{\partial (\log t)^2} \tag{13}$$

Equation 13 relates a concentration-dependent variable $\frac{\partial^2 \log L_d}{\partial (\log t)^2}$ to a structural variable $\frac{\partial^2 \log m}{\partial (\log t)^2}$. It implies that changes made in the arc length of displacement by PEGDA concentration are equally reflected at the microstructure level as the increasing rate of average mesh size. This statement is validated by comparing the concavities of the arc length of displacement $\left(\frac{\partial^2 \log L_d}{\partial (\log t)^2}\right)$ in Figure 14 with the concavities of average mesh size $\left(\frac{\partial^2 \log m}{\partial (\log t)^2}\right)$ in Figure 10, where good agreements are observed. By connecting the arc length of displacement with the average mesh size, shear-thickening behavior in hydrogels is explained. In lower-PEGDA-concentration hydrogels, the momentum diffusion exponents are larger. Therefore, the arc length of displacement increases faster. According to eq 13, this leads to higher rates of increase in average mesh size, which results in higher shear-thickening behavior.

6. SUMMARY

Nonequilibrium MD simulations and experiments of shear deformation are conducted on PEGDA hydrogels to study the rheological properties in transient-state Couette flow conditions. Hydrogels with 20, 25, 50, and 70 wt % PEGDA concentrations are used to investigate the influence of polymer concentration on the shear-thickening behavior in the transient state. The transient shear response of hydrogels is characterized by the self-similar solution and power-law fluid model. Both the shear-thickening exponent and viscous coefficient in the power-law fluid model are found to increase as PEGDA concentration decreases, which indicates higher shear-thickening behavior in lower-PEGDA-concentration hydrogels. Dimensionless variables are introduced to characterize the transient-state viscous properties of hydrogels regardless of the magnitude of acceleration.

To bridge the gap between simulation and experimental time scales, high strain rate simple shear experiments are conducted using a split-Hopkinson pressure bar apparatus, which imparts a linear velocity input to a hydrogel specimen. Displacement fields measured using 2D DIC allow for the computation of the shear-thickening exponent and transient-state viscosity. The experimental shear-thickening exponents show good agreement with the simulation results. In addition, the transient-state viscosity extrapolated from MD simulation is in agreement with the experimental results at their time scale.

The average mesh size and junction separation distribution are calculated from MD simulations to investigate shear-thickening mechanisms. Two stages of deformation in PEGDA chains are identified, where the first stage is associated with conformational changes and the second stage exhibits bond and angular changes. Additionally, the relationship between the network structure and polymer concentration is explored during transient-state deformation by introducing the arc length of displacement and the cumulative mesh size. Since the introduced variables are shown to be equal, as expected, the average mesh size is related to the arc length of displacement with the same concavity, which implies that the PEGDA concentration affects the increasing rate of average mesh size by the momentum diffusion exponent. Hydrogels with lower PEGDA concentration have a larger momentum diffusion exponent, which leads to a faster increase in mesh size. This results in increased resistance of PEGDA chains in both deformation stages and higher shear-thickening behavior.

The above results show that the polymer concentration has a major influence on the shear-thickening behavior of PEGDA hydrogels in the transient-state deformation regime via changes in the momentum diffusion exponent and the subsequent changes in mesh size. The results presented in this study are the first to directly relate the microstructure of the hydrogel with transient-state shear-thickening behavior and provide insights to develop the fundamental understanding of transient-state behavior in soft materials at high strain rates.

AUTHOR INFORMATION

Corresponding Author

*E-mail: dspearot@ufl.edu. Tel.: 352-392-6747.

ORCID

Ghatu Subhash: 0000-0002-5996-0909

Douglas E. Spearot: 0000-0003-1875-6036

Notes

The authors declare no competing financial interest.

ACKNOWLEDGMENTS

This work was supported by the National Science Foundation under Grant Nos. CMMI-1634188 and CMMI-1762791. The authors acknowledge the University of Florida Research Computing for providing computational resources. The authors thank Professor Thomas Angelini and Ph.D. student Cameron Morley for providing support in the preparation of PEGDA samples.

DOI: 10.1021/acs.macromol.9b00820
Macromolecules 2019, 52, 5860–5871

REFERENCES

(1) Peppas, N. A. *Hydrogels in Medicine and Pharmacy: Properties and Applications*; Peppas, N. A., Ed.; CRC Press: The University of Michigan, 1987; Vol. 3.

(2) El-Sherbiny, I. M.; Yacoub, M. H. Hydrogel Scaffolds for Tissue Engineering: Progress and Challenges. *Glob. Cardiol. Sci. Pract.* **2013**, *2013*, No. 38.

(3) Drury, J. L.; Mooney, D. J. Hydrogels for Tissue Engineering: Scaffold Design Variables and Applications. *Biomaterials* **2003**, *24*, 4337−4351.

(4) Zhao, X.; Sun, X.; Yildirimer, L.; Lang, Q.; Lin, Z. Y.; Zheng, R.; Zhang, Y.; Cui, W.; Annabi, N.; Khademhosseini, A. Cell Infiltrative Hydrogel Fibrous Scaffolds for Accelerated Wound Healing. *Acta Biomater.* **2017**, *49*, 66−77.

(5) Haryanto; Kim, J. H.; Kim, J. O.; Ku, S.; Cho, H.; Han, D. H.; Huh, P. Fabrication of Poly(Ethylene Oxide) Hydrogels for Wound Dressing Application Using E-Beam. *Macromol. Res.* **2014**, *22*, 131−138.

(6) Subhash, G.; Kwon, J.; Mei, R.; Moore, D. F. Non-Newtonian Behavior of Ballistic Gelatin at High Shear Rates. *Exp. Mech.* **2012**, *52*, 551−560.

(7) Anseth, K. S.; Bowman, C. N.; Brannon-Peppas, L. Mechanical Properties of Hydrogels and Their Experimental Determination. *Biomaterials* **1996**, *17*, 1647−1657.

(8) Oosten, A. S.; van Galie, P. A.; Janmey, P. A. Mechanical Properties of Hydrogels. In *Gels Handbook: Fundamentals, Properties, Applications (In 3 Volumes)*; World Scientific, 2016; pp 67−79.

(9) Appleby-Thomas, G. J.; Hazell, P. J.; Sheldon, R. P.; Stennett, C.; Hameed, A.; Wilgeroth, J. M. The High Strain-Rate Behaviour of Selected Tissue Analogues. *J. Mech. Behav. Biomed. Mater.* **2014**, *33*, 124−135.

(10) Kwon, J.; Subhash, G. Compressive Strain Rate Sensitivity of Ballistic Gelatin. *J. Biomech.* **2010**, *43*, 420−425.

(11) Shepherd, C. J.; Appleby-Thomas, G. J.; Hazell, P. J.; Allsop, D. F.; Elert, M.; Furnish, M. D.; Anderson, W. W.; Proud, W. G.; Butler, W. T. The Dynamic Behavior of Ballistic Gelatin. *AIP Conf. Proc.* **2009**, *1195*, 1399−1402.

(12) Liu, Q.; Subhash, G. Characterization of Viscoelastic Properties of Polymer Bar Using Iterative Deconvolution in the Time Domain. *Mech. Mater.* **2006**, *38*, 1105−1117.

(13) Richler, D.; Rittel, D. On the Testing of the Dynamic Mechanical Properties of Soft Gelatins. *Exp. Mech.* **2014**, *54*, 805−815.

(14) Naarayan, S. S.; Subhash, G. Wave Propagation in Ballistic Gelatine. *J. Mech. Behav. Biomed. Mater.* **2017**, *68*, 32−41.

(15) Hoffman, R. L. Explanations for the Cause of Shear Thickening in Concentrated Colloidal Suspensions. *J. Rheol.* **1998**, *42*, 111−123.

(16) Cheng, X.; McCoy, J. H.; Israelachvili, J. N.; Cohen, I. Imaging the Microscopic Structure of Shear Thinning and Thickening Colloidal Suspensions. *Science* **2011**, *333*, 1276−1279.

(17) Ternik, P.; Marn, J.; Zunic, Z. Non-Newtonian Fluid Flow through a Planar Symmetric Expansion: Shear-Thickening Fluids. *J. Non-Newtonian Fluid Mech.* **2006**, *135*, 136−148.

(18) Zaman, A. A.; Bjelopavlic, M.; Moudgil, B. M. Effect of Adsorbed Polyethylene Oxide on the Rheology of Colloidal Silica Suspensions. *J. Colloid Interface Sci.* **2000**, *226*, 290−298.

(19) Cates, M. E.; Head, D. A.; Ajdari, A. Rheological Chaos in a Scalar Shear-Thickening Model. *Phys. Rev. E* **2002**, *66*, No. 025202.

(20) Head, D. A.; Ajdari, A.; Cates, M. E. Rheological Instability in a Simple Shear-Thickening Model. *Europhys. Lett.* **2002**, *57*, 120−126.

(21) Barbucci, R. *Hydrogels: Biological Properties and Applications*; Springer Science & Business Media, 2010.

(22) Yakimets, I.; Paes, S. S.; Wellner, N.; Smith, A. C.; Wilson, R. H.; Mitchell, J. R. Effect of Water Content on the Structural Reorganization and Elastic Properties of Biopolymer Films: A Comparative Study. *Biomacromolecules* **2007**, *8*, 1710−1722.

(23) Subhash, G.; Liu, Q.; Moore, D. F.; Ifju, P. G.; Haile, M. A. Concentration Dependence of Tensile Behavior in Agarose Gel Using Digital Image Correlation. *Exp. Mech.* **2011**, *51*, 255−262.

(24) Luo, K.; Yudewitz, N.; Subhash, G.; Spearot, D. E. Effect of Water Concentration on the Shock Response of Poly(ethylene glycol)diacrylate (PEGDA) Hydrogels: A Molecular Dynamics Study. *J. Mech. Behav. Biomed. Mater.* **2019**, *90*, 30−39.

(25) Kröger, M.; Loose, W.; Hess, S. Rheology and Structural Changes of Polymer Melts via Nonequilibrium Molecular Dynamics. *J. Rheol.* **1993**, *37*, 1057−1079.

(26) Jeng, Y.; Chen, C.; Shyu, S. A Molecular Dynamics Study of Lubrication Rheology of Polymer Fluids. *Tribol. Lett.* **2003**, *15*, 293−299.

(27) Cui, S. T.; Cummings, P. T.; Cochran, H. D. Molecular Dynamics Simulation of the Rheological and Dynamical Properties of a Model Alkane Fluid under Confinement. *J. Chem. Phys.* **1999**, *111*, 1273−1280.

(28) Cui, S. T.; Cummings, P. T.; Cochran, H. D. Molecular Simulation of the Transition from Liquidlike to Solidlike Behavior in Complex Fluids Confined to Nanoscale Gaps. *J. Chem. Phys.* **2001**, *114*, 7189−7195.

(29) Rapaport, D. C.; Rapaport, D. C. R. *The Art of Molecular Dynamics Simulation*; Cambridge University Press, 2004.

(30) Kwon, J.; Subhash, G.; Mei, R.; Heger, I. An Optical Technique for Determination of Rheological Properties of Gelatin. *J. Rheol.* **2011**, *55*, 951−964.

(31) Saramito, P. *Complex Fluids; Mathématiques et Applications*; Springer International Publishing: Cham, 2016; Vol. *79*.

(32) Harris, J. *Rheology and Non-Newtonian Flow*; Longman Publishing Group: London, 1977.

(33) Magyari, E.; Ali, M. E.; Keller, B. Heat and Mass Transfer Characteristics of the Self-Similar Boundary-Layer Flows Induced by Continuous Surfaces Stretched with Rapidly Decreasing Velocities. *Heat Mass Transf.* **2001**, *38*, 65−74.

(34) Magyari, E.; Keller, B. Exact Solutions for Self-Similar Boundary-Layer Flows Induced by Permeable Stretching Walls. *Eur. J. Mech. B Fluids* **2000**, *19*, 109−122.

(35) Ju, H.; McCloskey, B. D.; Sagle, A. C.; Kusuma, V. A.; Freeman, B. D. Preparation and Characterization of Crosslinked Poly(Ethylene Glycol) Diacrylate Hydrogels as Fouling-Resistant Membrane Coating Materials. *J. Memb. Sci.* **2009**, *330*, 180−188.

(36) Gabler, S.; Stampfl, J.; Koch, T.; Seidler, S.; Schuller, G.; Redl, H.; Juras, V.; Trattnig, S.; Weidisch, R. Determination of the Viscoelastic Properties of Hydrogels Based on Poly(ethylene glycol)Diacrylate (PEG-DA) and Human Articular Cartilage. *Int. J. Mater. Eng. Innov.* **2009**, *1*, 3−20.

(37) Witte, R. P.; Blake, A. J.; Palmer, C.; Kao, W. J. Analysis of Poly(Ethylene Glycol)-Diacrylate Macromer Polymerization within a Multicomponent Semi-Interpenetrating Polymer Network System. *J. Biomed. Mater. Res.* **2004**, *71*, 508−518.

(38) Jang, S. S.; Goddard, W. A.; Kalani, M. Y. S. Mechanical and Transport Properties of the Poly(Ethylene Oxide)−Poly(Acrylic Acid) Double Network Hydrogel from Molecular Dynamic Simulations. *J. Phys. Chem. B* **2007**, *111*, 1729−1737.

(39) Liew, C. C.; Inomata, H.; Arai, K. Flexible Molecular Models for Molecular Dynamics Study of near and Supercritical Water. *Fluid Phase Equilib.* **1998**, *144*, 287−298.

(40) Mattsson, T. R.; Lane, J. M. D.; Cochrane, K. R.; Desjarlais, M. P.; Thompson, A. P.; Pierce, F.; Grest, G. S. First-Principles and Classical Molecular Dynamics Simulation of Shocked Polymers. *Phys. Rev. B: Condens. Matter Mater. Phys.* **2010**, *81*, 1−9.

(41) Leng, Y.; Cummings, P. T. Fluidity of Hydration Layers Nanoconfined between Mica Surfaces. *Phys. Rev. Lett.* **2005**, *94*, No. 026101.

(42) Sun, D.; Zhou, J. Effect of Water Content on Microstructures and Oxygen Permeation in PSiMA−IPN−PMPC Hydrogel: A Molecular Simulation Study. *Chem. Eng. Sci.* **2012**, *78*, 236−245.

(43) Lee, H.; Venable, R. M.; MacKerell, A. D.; Pastor, R. W. Molecular Dynamics Studies of Polyethylene Oxide and Poly(ethylene glycol): Hydrodynamic Radius and Shape Anisotropy. *Biophys. J.* **2008**, *95*, 1590−1599.

DOI: 10.1021/acs.macromol.9b00820
Macromolecules 2019, 52, 5860−5871

(44) Wu, Y.; Joseph, S.; Aluru, N. R. Effect of Cross-Linking on the Diffusion of Water, Ions, and Small Molecules in Hydrogels. *J. Phys. Chem. B* **2009**, *113*, 3512−3520.
(45) Jewett, A.; Lambert, J. *Moltemplate*, 2014.
(46) Stringer, J. L.; Peppas, N. A. Diffusion of Small Molecular Weight Drugs in Radiation-Crosslinked Poly(Ethylene Oxide) Hydrogels. *J. Controlled Release* **1996**, *42*, 195−202.
(47) Flory, P. J.; Rehner, J. Statistical Mechanics of Cross-Linked Polymer Networks I. Rubberlike Elasticity. *J. Chem. Phys.* **1943**, *11*, 512−520.
(48) Yong, X.; Zhang, L. T. Examining Different NEMD Methods in Simulating Nanoscale Fluid at High Shear Rates. *Proc. Inst. Mech. Eng., Part N* **2010**, *224*, 19−29.
(49) Plimpton, S. Fast Parallel Algorithms for Short-Range Molecular Dynamics. *J. Comput. Phys.* **1995**, *117*, 1−19.
(50) Upadhyay, K.; Bhattacharyya, A.; Subhash, G.; Spearot, D. E. Quasi-Static and High Strain Rate Simple Shear Characterization of Soft Polymers. *Exp. Mech.* **2019**, 1−15.
(51) Likhachev, E. R. Dependence of Water Viscosity on Temperature and Pressure. *Tech. Phys.* **2003**, *48*, 514−515.
(52) Long, D.; Sotta, P. Numerical Simulation for the Mesoscale Deformation of Disordered Reinforced Elastomers. In *Modeling of Soft Matter*; Springer, 2005; pp 205−233.
(53) Zustiak, S. P.; Leach, J. B. Hydrolytically Degradable Poly(Ethylene Glycol) Hydrogel Scaffolds with Tunable Degradation and Mechanical Properties. *Biomacromolecules* **2010**, *11*, 1348−1357.
(54) Lin, H.; Kai, T.; Freeman, B. D.; Kalakkunnath, S.; Kalika, D. S. The Effect of Cross-Linking on Gas Permeability in Cross-Linked Poly(Ethylene Glycol Diacrylate). *Macromolecules* **2005**, *38*, 8381−8393.
(55) Hojjat, M.; Etemad, S. G.; Bagheri, R.; Thibault, J. Rheological Characteristics of Non-Newtonian Nanofluids: Experimental Investigation. *Int. Commun. Heat Mass Transf.* **2011**, *38*, 144−148.
(56) Yang, T. Mechanical and Swelling Properties of Hydrogels. Doctoral Dissertation, KTH Royal Institute of Technology, 2012.
(57) Lee, S. G.; Brunello, G. F.; Jang, S. S.; Bucknall, D. G. Molecular Dynamics Simulation Study of P (VP-Co-HEMA) Hydrogels: Effect of Water Content on Equilibrium Structures and Mechanical Properties. *Biomaterials* **2009**, *30*, 6130−6141.
(58) Davison, L.; Horie, Y.; Graham, R. A. *Shock Wave and High Pressure Phenomena*; Ben-Dor, G., Lu, F. K.., Thadhani, N. D., Horie, Y., Eds.; Springer, 2008.
(59) Heymann, B.; Grubmüller, H. Elastic Properties of Poly-(Ethylene-Glycol) Studied by Molecular Dynamics Stretching Simulations. *Chem. Phys. Lett.* **1999**, *307*, 425−432.

DOI: 10.1021/acs.macromol.9b00820
Macromolecules 2019, 52, 5860−5871